

Boris Epel · Kai-Oliver Schäfer · Armin Quentmeier
Cornelius Friedrich · Wolfgang Lubitz

Multifrequency EPR analysis of the dimanganese cluster of the putative sulfate thiohydrolase SoxB of *Paracoccus pantotrophus*

Received: 17 December 2004 / Accepted: 26 July 2005 / Published online: 31 August 2005
© SBIC 2005

Abstract A detailed analysis of the EPR signatures at X-band and Q-band of an enzyme (SoxB) involved in sulfur oxidation from *Paracoccus pantotrophus* is presented. EPR spectra are attributed to an exchange-coupled dimanganese Mn₂(II,II) complex. An antiferromagnetic exchange interaction of $J = -7.0 (\pm 1) \text{ cm}^{-1}$ ($H = -2JS_1S_2$) is evidenced by a careful examination of the temperature dependence of the EPR spectra. The spin Hamiltonian parameters for a total spin of $S^T = 1, 2$ and 3 are obtained and an inter-manganese distance of 3.4 (± 0.1) Å is estimated. The comparison with exchange coupling and inter-manganese distance data of other dimanganese proteins and model compounds leads to a tentative assignment of the Mn bridging ligands to bis(μ -hydroxo) (μ -carboxylato).

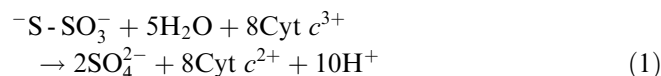
Keywords Sulfate thiohydrolase · Manganese protein · *Paracoccus pantotrophus* · Electron paramagnetic resonance · Magnetic exchange

Introduction

Oxidation of inorganic sulfur compounds to sulfuric acid represents the oxidative half of the global sulfur cycle. Sulfur oxidation is performed by aerobic chemo-

trophic and anaerobic phototrophic prokaryotes. In *Paracoccus (P.) pantotrophus* the sulfur oxidizing (Sox) enzyme system is located in the periplasm. Four soluble proteins, SoxXA, SoxYZ, SoxB, and SoxCD constitute the sulfur-oxidizing enzyme system in vitro. This system mediates hydrogen sulfide-, sulfur-, thiosulfate-, and sulfite-dependent cytochrome *c* reduction. Each of the proteins alone is catalytically inactive [1].

The material balance of thiosulfate oxidation by this system is given by.



According to the current model [2, 3] thiosulfate is covalently bound by the heme enzyme complex SoxXA to the thiol of the cysteine residue of the SoxY protein to form cysteine-thiosulfonate (Fig. 1). The sulfonate moiety is proposed to be hydrolyzed off by the dimanganese SoxB protein to yield SoxY-cysteine persulfide.

The primary structure of SoxB is about 30% identical to zinc-containing 5'nucleotidases from various sources (see e.g. Ref. [4]). Since, however, the features of the primary structure are clearly distinct from the 5'nucleotidases, none of the Sox proteins is phosphorylated and phosphate is not involved in the reaction cycle, SoxB is proposed to act as thiosulfate hydrolase releasing sulfate and SoxY-cysteine persulfide [3]. The outer sulfur atom (the sulfane sulfur) of SoxY-cysteine persulfide is then oxidized by the molybdoprotein cytochrome complex sulfur dehydrogenase Sox(CD)₂, and the sulfonate moiety is again hydrolyzed off by the sulfatase SoxB. The monomeric SoxB protein contains two manganese atoms, pyroglutamate (cyclo-glutamate) as N-terminus and the predicted molecular mass (58,611Da) is identical to that determined by electrospray mass spectrometry [1, 5].

Manganese ions are paramagnetic and EPR spectroscopy can provide information on the number of Mn ions, their distance and oxidation states [6]. Further-

B. Epel · W. Lubitz (✉)
Max-Planck-Institut für Bioanorganische Chemi,
Stiftstr. 34-36, 45470 Mülheim, Ruhr, Germany
E-mail: lubitz@mpi-muelheim.mpg.de
Fax: +49-208-3063955

K.-O. Schäfer
Max-Volmer-Laboratorium für Biophysikalische Chemie,
Technische Universität Berlin, PC14, Strasse des 17. Juni 135,
10623 Berlin, Germany

A. Quentmeier · C. Friedrich
Lehrstuhl für Technische Mikrobiologie,
Fachbereich Chemietechnik, Universität Dortmund,
Emil-Figge-Strasse 66, 44221 Dortmund, Germany

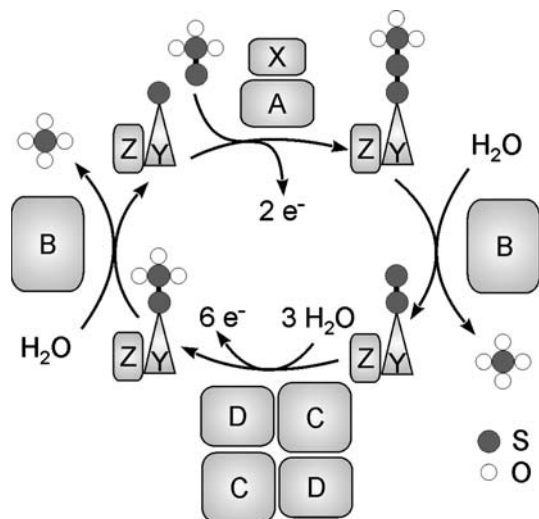


Fig. 1 Proposed model for the mechanism of chemotrophic thiosulfate oxidation of the sulfur-oxidizing enzyme system of *P. pantotrophus* (for details see Ref. [3]). SoxB catalyzes the hydrolytic cleavage of sulfate from cysteine thiosulfonate of SoxY to cysteine persulfide (right side) and the one from cysteine sulfonate of SoxY to regenerate SoxY (left side). Closed circles represent sulfur atoms and open circles represent oxygen atoms.

more, the magnitudes of the Mn–Mn Heisenberg spin exchange and magnetic dipole–dipole interactions, the spin multiplicity of the lowest electronic states, and the spatial symmetry of the Mn ligand field can be obtained. The first EPR observation of a SoxB protein was reported by Cammack et al. [7] for *Thiobacillus versutis*. In this work, the spectrum was attributed to an equal valence $Mn_2(II,II)$ pair and the similarity between the EPR spectra of SoxB and selected model compounds was discussed. An analysis of EPR parameters was not performed.

The EPR spectra of proteins [6] as well as synthetic complexes [8, 9] containing a manganese dimer in the $Mn_2(II,II)$ oxidation state are generally complex, with several of the five electronic states (total spin $S^T = 1, \dots, 5$) contributing to the spectrum at elevated temperatures, owing to the small energy separations between the states. The EPR spectra of these states overlap, making a separation and analysis of the ^{55}Mn hyperfine splittings (HFS) and zero-field splittings (ZFS) very complicated. However, a simulation of the spectra is often possible with a sufficient precision [10], especially for the low-lying electronic states [11, 12].

In this communication the EPR spectra of the dimanganese SoxB protein both at 9.6 and 34 GHz microwave frequencies are reported at various temperatures. The resolved lines in the EPR spectra originate from transitions attributed to a total spin $S^T = 1, 2, 3$ states of the exchange-coupled system. The comparison of the spin Hamiltonian parameters of SoxB dimanganese proteins with model compounds with known structure allows an estimation of the distance between the Mn(II) ions and leads to a proposal of a putative structure of the complex.

Materials and methods

Sample preparation

The SoxB protein of *P. pantotrophus* was purified to homogeneity as previously described [1]. The homogeneous enzyme (20 mg/ml) was dissolved in a 10 mM Tris/HCl buffer, pH 7.5, with 2 mM $Na_2S_2O_3$, 1 mMol/l $MgSO_4$ and 1 μ M phenylmethylsulfonylfluoride (PMSF) and stored in liquid nitrogen. These conditions maintained the catalytic activity of SoxB within the reconstituted sulfur-oxidizing enzyme system [1]. The final preparation of samples for the EPR measurements was done under an argon atmosphere.

Spectroscopic measurements

Continuous wave (cw) X-band (9.6 GHz) measurements (perpendicular mode) were carried out by using a Bruker Elexsys 500 spectrometer with a rectangular dual mode cavity ER 4116 DM and an Oxford helium flow cryostat ER 910. For the respective Q-band (34 GHz) measurements an ESP 300 E spectrometer with an ER 5106 QT cylindrical cavity and Oxford helium flow cryostat CF 935 were employed. A modulation frequency of 100 kHz with 1 mT amplitude was used for all measurements. All experiments were performed under non-saturating conditions. The calibration of the temperature was done before the experiment using a calibrated thermocouple placed inside the sample tube. The precision of temperature measurements is better than 0.5 K at $T < 15$ K and 2 K at higher temperatures.

Simulation and data processing

The EPR simulations were performed using XSophe software developed by the department of Mathematics at the University of Queensland, Brisbane (Australia) for Bruker Biospin GmbH [13] and EasySpin software package by Physical Chemistry Laboratory at ETH Honggerberg, Zurich (Switzerland) [14] as well as home written routines. The data processing was done in MatlabTM [15]. The data traces that present the extracted hyperfine structure were produced by subtraction of the broad part of the EPR spectra, which was obtained by filtering out the sharp features using the Savitzky–Golay method [15]. For all simulations Lorentzian line shapes were used.

Theory

The full spin Hamiltonian for an exchange-coupled two-spin system can be written as [16]:

$$H = -2J\vec{S}_1\vec{S}_2 + \vec{S}_1\mathbf{d}_{12}\vec{S}_2 + \sum_{i=1,2} \left(\vec{S}_i\mathbf{d}_i\vec{S}_i + \mu_B\vec{B}_0\mathbf{g}_i\vec{S}_i + \vec{I}_i\mathbf{a}_i\vec{S}_i \right) \quad (2)$$

where the first term is the Heisenberg exchange. The sign of the exchange coupling integral is strongly dependent on the coordination, in particular on the bridging situation of the ions. It can be positive (ferromagnetic) or negative (antiferromagnetic) depending on the spatial structure of the electronic wavefunction of the system. In this article, we consider only the isotropic part of the exchange coupling tensor J , because the anisotropic part is typically small and it is complicated to evaluate from EPR data.

The second term in Eq. 2 is the magnetic dipolar coupling. Dipolar coupling mainly depends on the distance between paramagnetic centers. Using the point-dipole approximation the tensor \mathbf{d}_{12} can be expressed as

$$\mathbf{d}_{12} = \frac{\mu_B^2}{r^3} \left(\mathbf{g}_1\mathbf{g}_2 - \frac{3(\mathbf{g}_1\vec{r})(\vec{r}\mathbf{g}_2)}{r^2} \right), \quad (3)$$

where \vec{r} is a distance vector between two ions and \mathbf{g}_1 and \mathbf{g}_2 are the g -factors of the two ions.

The last term of Eq. 2 contains the sum of the spin Hamiltonians of the single ions, namely the zero-field splitting, electronic Zeeman interaction, and hyperfine coupling terms, respectively. The nuclear Zeeman interaction is neglected because it does not contribute to the allowed EPR transitions. The zero-field tensor is traceless and can be presented in the form:

$$\hat{S}\mathbf{d}\hat{S} = D \left[\hat{S}_z^2 - \frac{1}{3}S(S+1) \right] + E \left[\hat{S}_x^2 - \hat{S}_y^2 \right], \quad (4)$$

where D and E describe the axial and non-axial parts of the zero-field splitting tensor, respectively.

Based on the spectral appearance it is assumed that the SoxB enzyme contains a $\text{Mn}_2(\text{II},\text{II})$ oxidation state. Other possible equal valence states, that is, $\text{Mn}_2(\text{III},\text{III})$ and $\text{Mn}_2(\text{IV},\text{IV})$, are known to exhibit very high ZFS single ion values, leading to difficulties in the observation of such spectra. The ZFS of the Mn(II) ion is typically smaller than 0.1 cm^{-1} [17]. The single ion Mn(II) has the electronic configuration $3d^5$ and electron spin $S=5/2$. There is only one natural manganese isotope (^{55}Mn) with a nuclear spin of $I=5/2$. For ion pairs with the exchange interaction J significantly larger than the other interactions (strong exchange limit) it is possible to use the Hamiltonian in total spin representation and separately analyze EPR spectra originating from states with different total spin momentum [16]. As will be shown later the exchange coupling J for the SoxB complex is about -7 cm^{-1} . The Zeeman interaction is smaller than 1.2 cm^{-1} in the present study. Therefore, one can treat the Hamiltonian in the strong exchange limit and the spin states can be described by total spin quantum numbers ranging from $|S_1 - S_2|$ to $|S_1 + S_2|$. The antiferromagnetic ($J < 0$) exchange coupling shifts

the levels with different projections of the total spin producing a ‘‘ladder’’ of spin states, with total spin $S^T = 0, 1, 2, 3, 4$, and 5 in order of increasing energy. Due to different Boltzmann populations, these spin states do not contribute equally to the resulting spectrum at a particular temperature. The Boltzmann coefficients describing the population of the single Zeeman level of the spin state S^T at thermal equilibrium and zero field are given by Eq. 5 [16]:

$$n_{s^T}(J, T) = \frac{\exp(-S^T(S^T + 1)J/kT)}{\sum (2S_i^T + 1) \exp(-S_i^T(S_i^T + 1)J/kT)}. \quad (5)$$

As is evident from the above equation, at very low temperature ($kT \ll J$) only the $S^T = 0$ state is populated and hence no EPR signal is observed. Upon increasing the temperature, the other states gradually become populated and contribute to the EPR spectra. At high temperature ($kT \gg J$) a superposition of signals originating from all states is observed.

The Hamiltonian of the state S^T in a spin-coupled basis can be expressed as [16]:

$$H(S^T) = \vec{S}^T \mathbf{D}(S^T) \vec{S}^T + \mu_B \vec{B}_0 \mathbf{G} \vec{S}^T + \sum_{i=1,2} \vec{I}_i \mathbf{A}_i \vec{S}^T. \quad (6)$$

The parameters of the Hamiltonian $H(S^T)$ (Eq. 6) are related to the parameters of the spin Hamiltonian H (Eq. 2) by

$$\mathbf{G} = c_1\mathbf{g}_1 + c_2\mathbf{g}_2, \quad (7)$$

$$\mathbf{A}_i = c_i\mathbf{a}_i, \quad (8)$$

$$\mathbf{D}(S^T) = d_1\mathbf{d}_1 + d_2\mathbf{d}_2 + d_{12}\mathbf{d}_{12} \quad (9)$$

The c_i and d_i coefficients can be easily calculated (coefficients are tabulated in Ref. [16]). For an equal valence pair the c_i coefficients are equal to 1/2 and d_1 is equal to d_2 . Two coupled Mn nuclei with spin 5/2 produce a pattern with 4 $I+1=11$ hyperfine lines with relative intensities of 1:2:3:4:5:6:5:4:3:2:1, which can be used as a fingerprint for an equal valence pair.

Hamiltonian (2) contains more than 30 independent parameters. To simplify the problem the following assumptions were made: (i) the contributions of the two Mn ions to the g -factor (7) and ZFS (9) cannot be mathematically distinguished. Thus, both ions have identical parameters. The angle between the largest principal component of the sum of the single ion ZFS values and the Mn–Mn distance vector $r_{\text{Mn–Mn}}$ is θ . The azimuthal angle is not considered. (ii) The g -factor is isotropic. Consequently, the dipolar tensor (3) is axial and its largest component is collinear to $r_{\text{Mn–Mn}}$. (iii) The hyperfine coupling tensor \mathbf{a} is isotropic. Accordingly, only seven parameters were considered in the simulations: the inter-manganese distance $|r_{\text{Mn–Mn}}|$, the isotropic exchange coupling J ; the isotropic g -factor g ; the single ion Mn ZFS parameters D , E ; the angle θ ; and the isotropic hyperfine coupling a_{iso} .

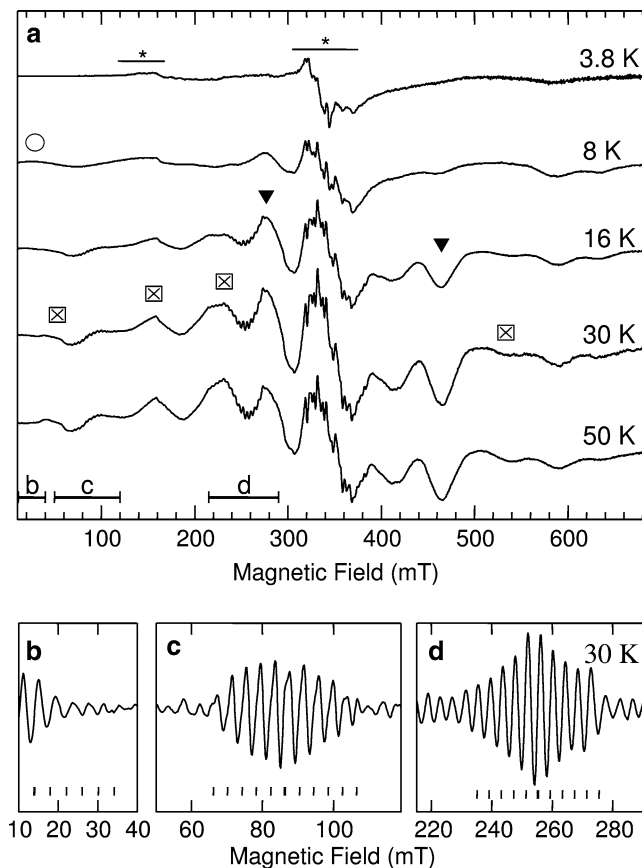


Fig. 2 **a** Experimental X-band spectra recorded at different temperatures. Microwave frequency $\nu = 9.6454$ GHz, microwave power 40 mW, and modulation amplitude 1 mT. The range of the impurity signals (at 3.8 K) are indicated and marked with asterisks. Features originating from spin states $S^T = 1$ (\circ), $S^T = 2$ (\blacktriangledown), and to $S^T = 3$ (\boxtimes) are marked with the corresponding symbols for those lines which were used for the temperature plot in Fig. 4. **b-d** Extracted hyperfine patterns at the selected regions of the spectrum **a** recorded at $T = 30$ K. The procedure is explained in the Materials and methods section. The 11-line patterns (split by 4.05 mT) are indicated by vertical bars at the bottom of the figure (**b-d**)

Results and discussion

Spectroscopic results

X-band EPR spectra

A selected set of X-band CW EPR spectra obtained at different temperatures is shown in Fig. 2. All spectra were measured using the same settings of the spectrometer. The spectral amplitudes were multiplied with an instrumental factor to correct the dependence of the signal amplitude on temperature due to the change of spectrometer parameters. A square-root dependence of the signal intensity on the microwave power at a temperature of 10 K was found up to the maximum available power of 200 mW, that is, the signals cannot be saturated. The spectrum at $T = 3.8$ K effectively exhibits signals solely originating from impurities (marked by

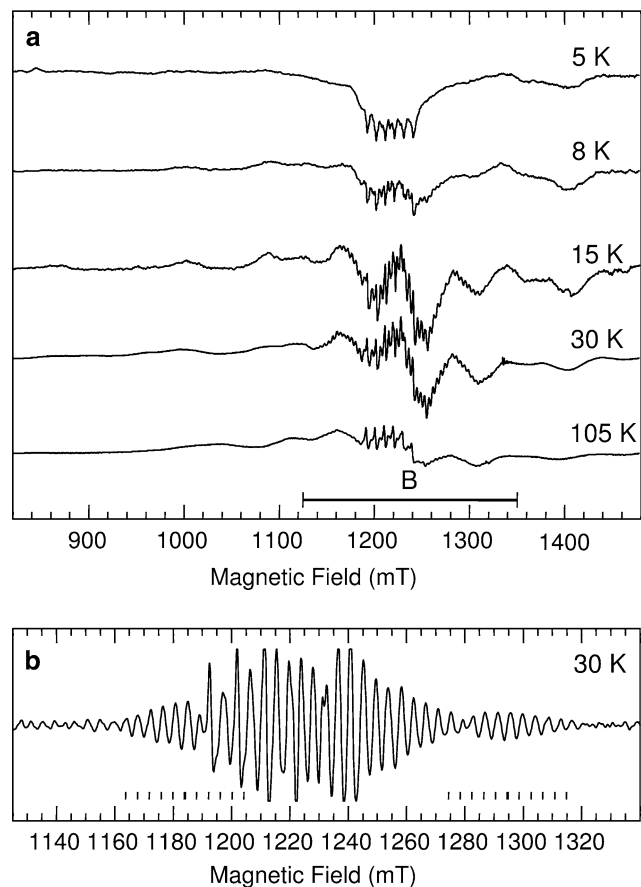


Fig. 3 **a** Experimental Q-band EPR spectra recorded at different temperatures. Microwave frequency $\nu_{mw} = 33.984$ GHz, microwave power 4 mW, modulation amplitude 1 mT. **b** Extracted hyperfine pattern from the central region of the spectrum recorded at $T = 30$ K. The 11-line patterns, which show a splitting of 4.1 mT, are indicated at the bottom of the figure

asterisks). These are assigned to monomeric Mn^{2+} ions, which show six distorted lines around 340 mT at $g = 2$ from the $| -1/2 \rangle \rightarrow | 1/2 \rangle$ transition. The relative amplitude of this signal varies depending on the preparation. The decrease of the microwave power by 50 dB leads to desaturation of the signal, it then shows the Curie temperature dependence. The signal near 150 mT ($g = 4.35 - 5.0$) results presumably from some Fe^{3+} impurity. With increasing temperature, new features appear in the range from 10 mT to 600 mT. Above 50 K, the spectra do not change significantly (data not shown). It was observed that there is a broad background above 40 K, which has a Gaussian line shape with a width of approximately 220 mT, presumably originating from high-spin transitions of the monomeric Mn^{2+} impurity and/or high-spin states of the dimanganese cluster. Careful inspection of the spectra shows that there are multiple sets of eleven lines split by 4.06 ± 0.05 mT observed in all traces above 6 K. The splitting slightly varies across the spectra indicating some hyperfine tensor anisotropy. The most prominent hyperfine patterns extracted from the spectrum at

Table 1 Parameters used for simulation of the EPR spectra

J^a (cm ⁻¹)	-7(±1)
g -factor	1.99(1)
a_{iso} (mT) _{<i>s</i>}	8.12(±0.1)
r_{Mn-Mn} (Å)	3.4(±0.1)
D (cm ⁻¹)	-0.09
E/D	0
θ (°)	15

$$^a H = -2 JS_1 S_2$$

$T=30$ K are presented in Fig. 2b–d. The intensity of these patterns is growing with temperature and reaches a maximum around $T=20$ K.

Q-band EPR spectra

The Q-band spectra of SoxB are shown in Fig. 3a. All amplitudes of the spectra are corrected as described for X-band. The spectra exhibit no features below 800 mT. The strong signals of the monomeric Mn²⁺ impurity (six-line pattern) at $B_0=1217$ mT (g -factor close to 2) are observed as in the X-band spectra. At a temperature of 5 K the spectra exhibit two broad transitions with a small intensity at 1010 mT and 1310 mT. At higher temperature, new features appear in the range between 1000 mT and 1500 mT. The spectrum at $T=105$ K has two additional features at 1034 mT and 1384 mT. The central regions of the spectra show overlapping 11-line hyperfine structures split by 4.12 ± 0.08 mT above 8 K. At a temperature of 30 K the amplitude of the hyperfine lines reaches its maximum. As in the X-band spectra above 30 K, a contribution of a broad background signal is observed.

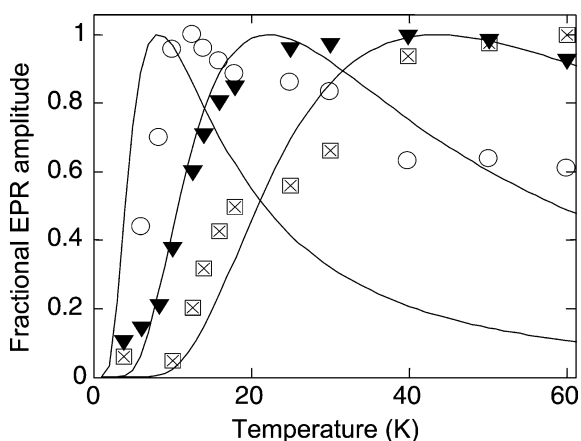


Fig. 4 Temperature dependence of selected spectral features originating from spin states $S^T = 1$ (○), $S^T = 2$ (▼ at 280 mT), and $S^T = 3$ (⊠ at 540 mT) at X-band (see Fig. 2). The temperature dependence of a particular spin state at different field positions indicated in Fig. 2 was very similar. The normalized population factors divided by the temperature, calculated according to Eq. 5 using $J = -7$ cm⁻¹ are plotted for comparison (solid lines)

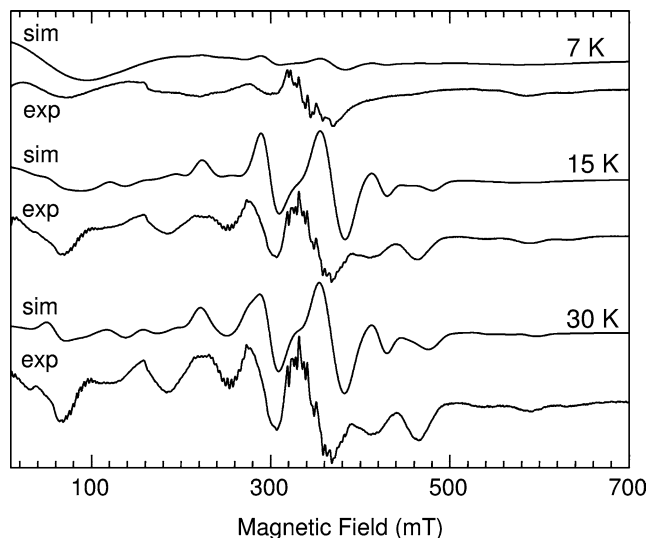


Fig. 5 Simulation of the X-band spectra at different temperatures. The parameters of the Hamiltonian (6) in a spin-coupled basis used for the simulation are $|D(S^T=1)| = 0.23$ cm⁻¹, $E(S^T=1)/D(S^T=1) = 0.27$, $|D(S^T=2)| = 0.07$ cm⁻¹, $E(S^T=2)/D(S^T=2) = 0.08$, $|D(S^T=3)| = 0.072$ cm⁻¹, $E(S^T=3)/D(S^T=3) = 0.06$; $J = -7$ cm⁻¹ and $G = 1.99$. The full-width at half-height linewidths are 120, 20, and 20 mT for spin states $S^T = 1, 2$ and 3, respectively. Final spectra are obtained by superposition of spectra originating from spin states $S^T = 1, 2$ and 3 with coefficients derived from Eq. 5

Data analysis

Two different approaches were used for spectral simulations. The first one is based on the direct solution of Hamiltonian (2) and accounts for the energy level population factors. However the direct solution of Hamiltonian (2), especially with the inclusion of the hyperfine terms, takes a very long computation time. Thus, for hyperfine structure simulations at Q-band and preliminary calculations, the routine based on perturbation treatment of the Hamiltonian (6) was used [17, 18]. The precision of the resonance field calculation of this routine is better than 0.3 mT.

The simultaneous fit of experimental data using the above-described model with seven independent parameters requires an automatic routine (see e.g. Ref. [10]). The quality of our data did not allow us to construct a good minimization function due to the strong impurity signal that obscures the central part of the spectra, especially at low temperatures. Thus, for the assignment of the spectral features, we first analyzed their temperature dependence, simulated features originating from spin states $S^T = 1$ (○), $S^T = 2$ (▼) and to $S^T = 3$ (⊠) and then used these results to estimate the parameters of the model. Figure 4 presents the normalized temperature dependence of selected spectral features in the X-band spectra (cf. Fig. 2). The amplitude of the features was calculated as a peak-to-peak difference. The normalized population factors divided by the temperature are plotted for

comparison (solid line). There are three different cases found. The feature around 50 mT shows the fastest growth with temperature with a maximum amplitude around 12 K. Thus, it was attributed to the $S^T = 1$ state. Features at 276 mT and 465 mT (\blacktriangledown) assigned to the $S^T = 2$ state show a slower growth and keep an almost constant amplitude between 30 K and 60 K. Lines at 40.7, 157.5 and 229.6 mT (\boxtimes) exhibit the slowest growth with temperature and are attributed to the $S^T = 3$ transition. Since no new features appear above $T=15$ K the higher spin states are assumed to be hidden in the broad background. A similar analysis of the Q-band spectra shows a less pronounced state separation due to significant overlap of spectral features originating from the states with different S^T .

Spectral simulations for the low temperature region comprising spin states $S^T = 1, 2$ and 3 at X and Q band are shown in Figs. 5 and 6, respectively. The simulation parameters are summarized in Table 1. In general the simulations of the Q-band spectra are found to be more reliable since at X-band the ZFS and Zeeman interaction terms in the spin Hamiltonian are very close to each other. This produces a very complicated pattern that is strongly dependent on small variations of the simulation parameters.

It is convenient to start with the analysis of spin state $S^T = 3$. For this state $d_{12} \gg d_1, d_2$ (Eq. 9), therefore $D(S^T = 3)$ is directly proportional to the dipolar term \mathbf{d}_{12} [19]. For typical inter-manganese distances of 3.2 Å to 4 Å the corresponding $|D(S^T = 3)|$ parameter will be equal to 0.08–0.04 cm^{-1} and the $E(S^T = 3)$ parameter is close to 0. From Fig. 4 it is evident that spin state $S^T = 3$ significantly contributes to the spectra recorded above 15 K as seen from the resolved hyperfine structure on the corresponding lines. The simulations show that the widths of the spectra at 15 K and 30 K and their major features are well reproduced by using $|D(S^T = 3)| = 0.07 \pm 0.005 \text{ cm}^{-1}$ and $E(S^T = 3) / |D(S^T = 3)| = 0.06 \pm 0.03$. The estimation of the corresponding inter-manganese distance using Eq. 3 yields values between 3.30 Å and 3.46 Å.

Based on the estimation of \mathbf{d}_{12} the other parameters of the model were tried to be fitted. The best simulation of all spectra was obtained with $D = -0.09 \text{ cm}^{-1}$, $E = 0$ and $\theta = 15^\circ$ (see Figs. 5, 6). Since not all spectra were reproduced well the mistake of determination of the single ion ZFS values D and E can be quite large. The value of the exchange coupling J used in the simulation is $-7 \pm 1 \text{ cm}^{-1}$. Although typically the values of exchange couplings derived from EPR data and other methods, for example, magnetization measurements [20], are in a good agreement, the proposed value has to be further verified.

The resolved hyperfine structure was found to originate only from the $S^T = 3$ state, while the features originating from the $S^T = 1$ state were found to be very broad. This implies a narrow distribution of inter-manganese distances and a broad distribution of single ion ZFS values, which contribute significantly to the

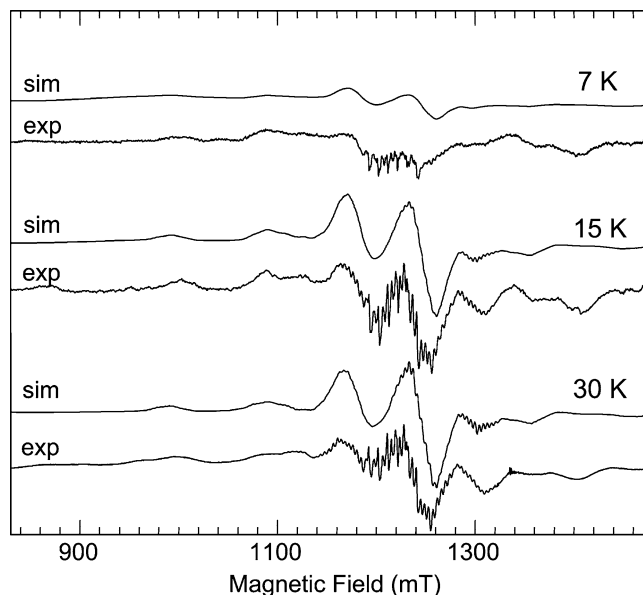


Fig. 6 Simulation of the Q-band spectra at different temperatures. The parameters of the Hamiltonian (6) in a spin-coupled basis used for the simulation are the same as for X-band (see Fig. 5); $A_{iso} = 4.06 \text{ mT}$. The full-width at half-height linewidths are 120, 20, and 3 mT for spin states $S^T = 1, 2$ and 3 respectively. Note that at Q-band the Mn hyperfine term was explicitly included in the simulations. Final spectra are obtained by superposition of spectra originating from spin states $S^T = 1, 2$ and 3 with coefficients derived from Eq. 5.

latter state. A more detailed analysis of the line broadening factors in exchange-coupled systems can be found in Ref. [10]. The obtained single ion ZFS is too small for the majority of known $\text{Mn}_2(\text{III,III})$ complexes but is typical for $\text{Mn}_2(\text{II,II})$ complexes [9]. Therefore a posteriori we confirm the assignment of our system to a $\text{Mn}_2(\text{II,II})$ state.

Structural interpretation

A rather large data bank of exchange couplings, ZFS parameters and inter-manganese distances obtained from corresponding oxidation states of manganese catalase [6] and various model compounds [9] has been accumulated during recent years. It was shown that most common motifs for manganese bridging in proteins are μ -oxo, μ -hydroxo, and μ -carboxylato ligands. Depending on the type and number of bridges the inter-manganese distance and exchange-coupling parameter vary. For example, the structures with tris μ -carboxylato bridges have typical distances $r_{\text{Mn-Mn}} > 4 \text{ \AA}$ and $|J| < 2 \text{ cm}^{-1}$, whereas μ -oxo bridges provide a tighter binding with $r_{\text{Mn-Mn}} < 3.5 \text{ \AA}$ and $|J| > 2 \text{ cm}^{-1}$ [9]. The values close to $r_{\text{Mn-Mn}} = 3.4 \text{ \AA}$ and $J = -7 \text{ cm}^{-1}$ obtained in this work were found in compounds with a bis(μ -hydroxo)(μ -carboxylato) bridging motif [21] (3.35 Å and $J = -7 \text{ cm}^{-1}$).

Summary and conclusion

We have presented a detailed analysis of the EPR signature of the SoxB protein from *Paracoccus pantotrophus*. EPR spectra were attributed to an exchange-coupled dimanganese complex. Both ions were found in the Mn(II) electronic state with $S_i = 5/2$ ($i = 1$ and 2). An antiferromagnetic exchange interaction was evidenced by careful examination of the temperature dependence of the EPR spectra. Fitting of this dependence led to a value of $J = -7.0 (\pm 1) \text{ cm}^{-1}$. The spectra recorded between 6 K and 30 K can be reproduced by a linear combination of temperature-independent spectra originated from states with total spin $S^T = 1$, $S^T = 2$ and $S^T = 3$. The weight factors of these follow the temperature dependence expected from the Boltzmann populations of the spin ladder. The use of two microwave frequencies gave supporting evidence to the proposed values.

Furthermore, a distance of $3.3 (\pm 0.1) \text{ \AA}$ between the two Mn ions has been estimated. A comparison with the exchange-coupling and inter-manganese distance data for dimanganese proteins and model compounds led to a tentative assignment of the Mn bridging ligands to bis(μ -hydroxo)(μ -carboxylato).

A further more detailed evaluation has to await a crystal structure of the SoxB protein and reliable quantum chemical calculations on $\text{Mn}_2(\text{II}, \text{II})$ complexes. Work along these lines is in progress in our laboratories.

Acknowledgments Financial support by the Max Planck Society and the Deutsche Forschungsgemeinschaft (Grant Fr318/8-1 to C. G. F. and LU 315/16-1,2) is gratefully acknowledged.

References

1. Friedrich CG, Quentmeier A, Bardischewsky F, Rother D, Kraft R, Kostka S, Prinz H (2000) *J Bacteriol* 182:4677–4687
2. Quentmeier A, Friedrich CG (2001) *FEBS Lett* 503:168–172
3. Friedrich CG, Rother D, Bardischewsky F, Quentmeier A, Fischer J (2001) *Appl Environ Microbiol* 67:2873–2882
4. Beese LS, Steitz TA (1991) *EMBO J* 10:25–33
5. Quentmeier A, Hellwig P, Bardischewsky F, Grelle G, Kraft R, Friedrich CG (2003) *Biochem Biophys Res Commun* 312:1011–1018
6. Dismukes GC (1996) *Chem Rev* 96:2909–2926
7. Cammack R, Chapman A, Lu WP, Karagouni A, Kelly DP (1989) *FEBS Lett* 253:239–243
8. Law NA, Caudle MT, Pecoraro VL (1999) In: Sykes AG (eds) *Advances in inorganic chemistry*, vol 46. Academic Press, New York, pp 305–440
9. Wu AJ, Penner-Hahn JE, Pecoraro VL (2004) *Chem Rev* 104:903–938
10. Golombek AP, Hendrich MP (2003) *J Magn Reson* 165:33–48
11. Khangulov SV, Pessiki PJ, Barynin VV, Ash DE, Dismukes GC (1995) *Biochemistry* 34:2015–2025
12. Blanchard S, Blondin G, Riviere E, Nierlich M, Girerd JJ (2003) *Inorg Chem* 42:4568–4578
13. Hanson GR, Noble CJ, Gates KE, Burrage K (2001) *J Inorg Biochem* 86:248–248
14. Stoll S (2003) *Spectral simulations in solid-state EPR*. PhD Thesis, ETH Zürich
15. MatlabTM The Mathworks Inc., Natick, MA, <http://www.mathworks.com>
16. Benchini A, Gatteschi D (1990) *EPR of exchange coupled systems*. Springer-Verlag, Berlin, Heidelberg
17. Dowsing RD, Gibson JF, Goodgame M, Hayward PJ (1969) *J Chem Soc A: Inorg Phys Theor* 187–193
18. Meirovitch E, Poupko R (1978) *J Phys Chem* 82:1920–1925
19. Blanchard S, Blain G, Riviere E, Nierlich M, Blondin G (2003) *Chem Eur J* 9:4260–4268
20. Le Pape L, Perret E, Michaud-Soret I, Latour JM (2002) *J Biol Inorg Chem* 7:445–450
21. Bossek U, Wieghardt K, Nuber B, Weiss J (1989) *Inorg Chim Acta* 165:123–129